

Conditioning on a Volatility Proxy Compresses the Apparent Timescale of Collective Market Correlation

Yuda Bi^{1,*} and Vince D. Calhoun^{1,2}

¹*Center for Translational Research in Neuroimaging and Data Science (TReNDS), Atlanta, Georgia 30303, USA*

²*Georgia State University, Georgia Institute of Technology,
and Emory University, Atlanta, Georgia 30303, USA*

(Dated: March 17, 2026)

We address the attribution problem for apparent slow collective dynamics: is the observed persistence intrinsic, or inherited from a persistent driver? For the leading eigenvalue fraction $\psi_1 = \lambda_{\max}/N$ of S&P 500 60-day rolling correlation matrices (237 stocks, 2004–2023), a VIX-coupled Ornstein–Uhlenbeck model reduces the effective relaxation time from 298 to 61 trading days and improves the fit over bare mean reversion by $\Delta\text{BIC}=109$. On the decomposition sample, an informational residual of $\log(\text{VIX})$ alone retains most of that gain ($\Delta\text{BIC}=78.6$), whereas a mechanical VIX proxy alone does not improve the fit. Autocorrelation-matched placebo fields fail ($\Delta\text{BIC}_{\max}=2.7$), disjoint weekly reconstructions still favor the field-coupled model ($\Delta\text{BIC}=140\text{--}151$), and six anchored chronological holdouts preserve the out-of-sample advantage. Quiet-regime and field-stripped residual autocorrelation controls show the same collapse of persistence. Stronger hidden-variable extensions remain only partially supported. Within the tested stochastic class, conditioning on the observed VIX proxy absorbs most of the apparent slow dynamics.

I. INTRODUCTION

A. Slow collective observables pose an attribution problem

Slow collective observables are routinely interpreted as evidence for intrinsic memory, metastability, or critical slowing down in complex systems [1–3]. The same empirical appearance can, however, arise when a moderately relaxing observable tracks an equilibrium that is itself displaced by a persistent external or latent field [4–7]. Distinguishing these two mechanisms is difficult whenever the field cannot be turned on and off experimentally, which is precisely the situation in ecological synchrony, dynamic brain connectivity, and climate variability [1, 2, 7]. The first logical task is therefore attribution: before positing intrinsic memory, one should ask whether the apparent persistence is inherited from the motion of a driver [4, 6, 8].

That attribution problem is sharper than a generic model-selection exercise [9, 10]. A slow observable can often be fit acceptably by several low-dimensional descriptions, including bare mean reversion, multistability, hidden-variable models, and explicit field-coupled dynamics [1, 5, 6]. Good in-sample fit alone therefore does not establish mechanism [9]. What is needed is a sequence of discriminations that asks which parts of the observed persistence survive conditioning, placebo substitution, and model-free controls [4, 7, 8]. The present manuscript is built around that sequence.

B. Financial correlation dynamics provide a stringent test case

Financial markets offer an unusually demanding testbed because they provide long, high-dimensional, and economically interpretable correlation time series [11–16]. Daily correlation matrices of large-cap U.S. equities exhibit a dominant market mode that is stable enough to track over decades and strong enough to matter for systemic-risk interpretation [11, 13, 17, 18]. At the same time, the candidate field proxy is not cleanly exogenous: volatility indices, realized co-movement, and broad risk sentiment are partly entangled by construction [19–22]. If an attribution workflow works here, it is likely to transfer to cleaner domains rather than only to easier ones.

The target of inference is therefore conditional attribution with respect to an observed field proxy, not proof of direct exogenous forcing [4, 9]. That distinction matters in finance because the strongest plausible confound is a latent common driver that moves both VIX and the collective correlation observable [19, 21]. The present design is built to separate intrinsic persistence, persistence-only surrogates, and purely mechanical overlap from that broader class of field-proxy explanations, while remaining explicit about what direct-coupling claims it cannot settle [8, 9].

The financial literature also supplies sharply competing narratives [23–27]. One strand emphasizes endogenous collective reorganization, cascade amplification, and near-critical dynamics [23–25, 28, 29]. Another strand emphasizes crisis-period heteroskedasticity, identifiable macro-financial shocks, and volatility-driven co-movement [17, 19–22]. These views need not be mutually exclusive, but they imply different expectations for the shape of the effective dynamics: intrinsic criticality points toward persistent double-well or memory-bearing structure, whereas field conditioning points toward a

* ybi3@gsu.edu

comparatively simple observable that relaxes around a moving equilibrium [1, 5, 6]. That distinction is exactly what the present tests are designed to probe.

Within that setting we study the leading-eigenvalue fraction

$$\psi_1(t) = \frac{\lambda_{\max}(t)}{\text{tr } C(t)} = \frac{\lambda_{\max}(t)}{N}, \quad (1)$$

where $C(t)$ is the rolling Pearson correlation matrix of stock returns. This quantity inherits the main intuition of random-matrix studies of financial correlation, namely that the dominant eigenmode captures collective market-wide alignment while the bulk largely reflects noise and sectoral substructure [11–14, 30]. It is also closely related to the absorption ratio and to state-classification approaches based on the correlation spectrum [18, 31–33]. What changes here is not the spectral object, but the question: rather than using the leading mode as a static diagnostic, we treat it as a dynamical variable whose persistence itself must be explained [34–37]. This choice is useful precisely because ψ_1 remains collective enough to track systemic episodes while remaining simple enough to admit explicit stochastic competition between field-free, field-coupled, and hidden-variable models [5, 6, 9, 17, 18, 31].

C. The literature gap is not whether memory exists, but what causes it

The immediate empirical background is the generalized-Langevin work of Wand, Heßler, and Kamps on the mean market correlation of the S&P 500 [38, 39]. Their results are important because they show that a one-dimensional memory-bearing description of collective market correlation is empirically viable and that the inferred memory kernel is not negligible [38, 40]. More broadly, they connect financial correlation dynamics to a growing literature on projected memory kernels and hidden slow variables in complex systems [4, 7, 41, 42]. But that approach leaves open a central causal question: does the apparent memory remain once explicit external fields are introduced and compared against persistence-matched placebo drivers [4, 8]?

That gap matters because several adjacent literatures already suggest that volatility conditions strongly modulate correlations during crises [19–22]. The options-implied volatility index VIX is especially relevant because it is persistent, forward-looking, and economically tied to broad uncertainty shocks [20, 21, 43]. At the same time, VIX is partly mechanical because both VIX and realized correlation respond to the same underlying return covariance matrix [19, 21]. A serious argument for field-driven dynamics must therefore do more than report a high correlation between VIX and ψ_1 . It must separate informational from mechanical overlap, show that persistence-matched surrogates fail, and test whether stronger hidden-variable interpretations still

add anything after the one-dimensional field problem has been settled [8, 9, 38].

Even then, a positive result against VIX should be read as evidence that an observed field proxy carries structured coupling information, not as proof that the proxy is the uniquely causal driver [4, 9, 19]. That is the inferential level at which the paper’s main claim is framed.

D. This paper provides a layered attribution test

The manuscript proceeds in three deliberately unequal layers. The first layer is the main result: we compare explicit one-dimensional stochastic models and show that conditioning on an observed VIX field proxy absorbs most of the apparent persistence in ψ_1 within the tested stochastic class, while autocorrelation-matched placebo fields fail by a wide margin. The second layer asks a harder question suggested by the generalized-Langevin literature: can the observed VIX itself serve as the hidden coordinate of an exact two-dimensional linear-Gaussian system whose projection generates memory [4, 7, 38, 40]? The third layer tests whether an orthogonal residual beyond VIX functions as a meaningful secondary order parameter or merely as a descriptive leftover [9, 44].

The evidential profile is intentionally asymmetric. The one-dimensional field-proxy attribution is strongly supported by formal model comparison, placebo rejection, directionality diagnostics, field decomposition, and model-free persistence collapse. The two-dimensional bridge survives only partially: it becomes more plausible under a Wand-faithful weekly construction, but it does not recover the reported memory scale cleanly. The orthogonal residual is descriptively nontrivial, but its forecasting role is not supported. This asymmetry is a feature rather than a flaw, because it keeps the strongest claim tied to the strongest evidence [9, 10].

The broader methodological point is transferable beyond finance. Any system that supplies a collective observable and a candidate field can be subjected to the same logic: build the collective variable, compare bare and field-coupled stochastic models, reject persistence-only surrogates in the spirit of surrogate-data testing, and only then move to stronger hidden-variable or residual-state interpretations [2, 7, 8, 45]. The rest of the paper follows that order. Section II details the data, experimental design, and estimation procedures used throughout. Section III presents the one-dimensional attribution result and its robustness tests, then the two-dimensional extension, and finally the orthogonal residual analysis. Section IV discusses what these results do and do not imply for collective market dynamics and for the broader study of apparent slow modes [1, 4, 38].

II. METHODS

A. Data, alignment, and construction of the collective observable

The daily baseline uses 237 S&P 500 constituents with continuous adjusted-close coverage from 2004 through 2023. Daily log returns are computed in the usual way, $r_i(t) = \log P_i(t) - \log P_i(t-1)$, and 60-trading-day rolling Pearson correlation matrices are formed from those returns, following the standard correlation-matrix construction used throughout the financial random-matrix literature [11–14]. The collective observable is the leading-eigenvalue fraction

$$\psi_1(t) = \frac{\lambda_{\max}(t)}{\text{tr} C(t)} = \frac{\lambda_{\max}(t)}{N}, \quad (2)$$

where $\text{tr} C = N$ because C is a Pearson correlation matrix with unit diagonal [11, 13, 15]. This observable is the dynamic analogue of the dominant market mode emphasized in random-matrix and absorption-ratio studies, but here it is treated as the dependent variable of a stochastic model rather than as a descriptive summary statistic [18, 31–33].

Daily VIX closing values are aligned to the same trading calendar using Federal Reserve Economic Data. After alignment, the one-dimensional SDE sample contains $n = 4973$ daily observations from 2004-03-30 through 2023-12-29. On that aligned sample, ψ_1 has mean 0.3778, standard deviation 0.1171, and maximum 0.7518 during the COVID-19 episode. These levels are not interpreted as thermodynamic invariants; they depend in part on the finite rolling-window estimator and on the high-dimensional aspect ratio of the correlation matrices [14, 15, 30].

The ratio $W/N = 60/237 \approx 0.25$ places each rolling correlation matrix in a regime where the Marchenko–Pastur bulk edge is nontrivial [14, 30]. That fact matters for level interpretation because the baseline value of ψ_1 contains a stationary noise-floor contribution from finite-sample eigenvalue spreading [14, 15]. It matters less for the present attribution exercise because the paper focuses on temporal comparisons—autocorrelation structure, model discrimination, and field conditioning—rather than on reading the absolute level of ψ_1 as a free-energy-like order parameter [9, 15, 16]. The same construction is recomputed directly from raw returns for $W = 30, 45, 60, 90, 120$ in the window-robustness experiment reported below and in Appendix C.

B. Experimental design and evidential logic

The empirical design is sequential rather than omnibus. Each stage is tied to a distinct rival explanation for the observed slowness of ψ_1 [4, 8, 9]. The primary comparison is between a bare OU model, which

attributes persistence to the observable itself, and a VIX-coupled OU model, which attributes part of that persistence to motion of a field-dependent equilibrium [5, 6, 21]. Quartic and regime-switching alternatives are then added to test whether the data favor endogenous multistability or rare discrete stress states over the continuous-field picture [23, 46, 47].

The main causal threat is that any sufficiently persistent driver might look good once inserted into the likelihood. We therefore define a formal placebo gate in which the real VIX field must beat 100 persistence-matched surrogate fields generated from the fitted marginal dynamics of $\log(\text{VIX})$ [8]. A second threat is circularity: VIX and ψ_1 are both functions of the same return covariance matrix. To address that concern we decompose VIX into mechanical and informational components, fit each component as a standalone field, and compare their model-selection power directly [9, 19, 21].

The design then moves outside the likelihood. Quiet-regime and field-stripped autocorrelation tests ask whether persistence still collapses when the field is approximately dormant or when the fitted conditional equilibrium is removed. The exact window-size sweep asks whether the field effect survives changes in time resolution. Disjoint weekly reconstructions and same-horizon disjoint 60-day blocks ask whether the core one-dimensional attribution survives once measurement overlap is reduced or removed. Anchored chronological hold-outs ask whether the main result is tied to one historical partition. MOVE and TED controls ask whether the field picture is broader than VIX, while the exact two-dimensional model asks whether the observed VIX can itself close the hidden-variable bridge suggested by generalized-Langevin work [7, 38, 40]. Finally, the orthogonal residual analysis tests whether a VIX-orthogonal state variable carries operational information beyond the main field story [44].

This layered design is deliberate. The paper’s strongest claim is attached to the largest evidential stack, not to the most ambitious theoretical extension [9, 10]. The robustness procedures are specified here and written out in execution detail in Appendix B so that the paper reads as a tightly linked sequence of discrimination tests rather than as a collection of disconnected checks.

The design also has a clear inference boundary. It can strongly distinguish bare intrinsic persistence from conditioning on an observed field proxy, and it can separately test autocorrelation-only and mechanical-overlap objections. It cannot, by itself, distinguish direct coupling from a latent common driver that moves both the proxy and the observable [4, 9, 19].

C. One-dimensional stochastic hierarchy and exact daily likelihood

The core model comparison is intentionally narrow. We test whether the daily dynamics of ψ_1 are better

TABLE I. Layered attribution logic. The strongest claim is the one that survives the largest stack of discrimination tests.

Rival explanation	Primary discrimination	Outcome in this manuscript
Bare intrinsic persistence or autocorrelation-only inheritance	M0 versus M2, placebo surrogates, quiet-regime ACF collapse, field-stripped residual ACF, disjoint weekly reconstructions, and anchored holdouts	Strongly disfavored
Purely mechanical overlap between VIX and ψ_1	Mechanical/informational decomposition, standalone field tests, and recipe sensitivity across freeze and weighting choices	Strongly disfavored dynamically
Observed VIX as the exact hidden coordinate behind projected memory	Exact two-dimensional linear-Gaussian comparison and projected-kernel timescale check	Only partially supported
VIX-orthogonal residual as an operational predictor	Q2-versus-Q3 future-VIX test across 30-, 60-, and 90-day horizons	Not supported

described by bare mean reversion, by mean reversion around a field-dependent equilibrium, or by simple non-linear alternatives often associated with metastability or effective double wells [1, 5, 6]. The two central models are

$$d\psi_1 = -\theta_0(\psi_1 - \mu_0) dt + \sigma_0 dW_t, \quad (3)$$

$$d\psi_1 = [-\theta(\psi_1 - \mu) + \beta v_t] dt + \sigma dW_t, \quad (4)$$

with $v_t = \log(\text{VIX}_t)$. The first model, M0, attributes all persistence to the observable itself. The second model, M2, allows the equilibrium to slide with the volatility field, so that $\mu_{\text{eff}}(v) = \mu + (\beta/\theta)v$ [5, 6, 21]. We also fit quartic-drift variants with and without the field, plus constrained two-state regime-switching competitors used only to calibrate whether a rare extreme-state channel adds structure beyond the continuous field [23, 46, 47].

For M0 and M2, the exact one-step Gaussian transition law is available in closed form because the drift is linear conditional on the field path. Treating v_t as piecewise constant over each daily interval, the exact daily transition is

$$\psi_{1,t+1} | \psi_{1,t}, v_t \sim \mathcal{N}(m_t, q), \quad (5)$$

with

$$m_t = e^{-\theta} \psi_{1,t} + (1 - e^{-\theta}) \left(\mu + \frac{\beta}{\theta} v_t \right), \quad (6)$$

$$q = \frac{\sigma^2}{2\theta} (1 - e^{-2\theta}), \quad (7)$$

and the obvious M0 specialization $\beta = 0$ [5, 6]. The exact derivation is given in Appendix A. We maximize the resulting Gaussian likelihood directly for M0 and M2. Quartic variants are optimized numerically under the same daily increment convention, and the constrained regime-switching models are estimated with a Gaussian Hamilton filter under a two-state Markov transition matrix [46, 47].

Model comparison is based on BIC, with AIC recorded as a secondary diagnostic. Because all fitted models are coarse-grained approximations to a far richer market process, the preferred specification is interpreted in

the pseudo-true sense of misspecified likelihood theory rather than as a literal data-generating law [9]. This point matters for the timescale language used later: the reported $\tau_{\text{auto}} = 1/\theta_0$ and $\tau_{\text{cond}} = 1/\theta$ are model-implied effective relaxation rates within the fitted OU class, not claims about a unique microscopic law [6, 9]. We also test a heteroskedastic variant M2', defined by the same OU+field drift as M2 but with

$$\sigma(\psi_1) = \sigma_0 + \sigma_1 \psi_1. \quad (8)$$

Because the diffusion coefficient is then state dependent, M2' is fit by direct numerical likelihood optimization under the same daily increment convention. Its role is diagnostic rather than headline: it asks whether modest state-dependent noise changes the field-attribution picture [6, 9]. Throughout the paper we summarize the model-based field contribution by

$$\text{SCPA} = 1 - \frac{\tau_{\text{cond}}}{\tau_{\text{auto}}} = 1 - \frac{\theta_0}{\theta}, \quad (9)$$

which compares the conditioned and bare OU timescales directly. We use the usual Jeffreys-style BIC scale only as an evidence summary, not as a substitute for robustness analysis [10]. The full execution details for the model-comparison pipeline are given in Appendix B.

D. Placebo gate and the formal attribution null

The strongest falsification device is a placebo-field gate modeled on surrogate-data logic [8]. We fit an AR(p) model to $v_t = \log(\text{VIX}_t)$, select p by AIC over $p = 1, \dots, 10$, and obtain $p = 9$ on the aligned sample. We then simulate 100 independent surrogate fields from that fitted marginal process and rescale each surrogate to the empirical mean and variance of the real series. Each surrogate then replaces the real VIX field in the same M2 likelihood. The formal null hypothesis is that the real VIX improvement can be matched by an independent realization drawn from the fitted AR marginal law of $\log(\text{VIX})$. Under that null, any large BIC gain would be attributable to generic persistence alone rather than

to specific coupling information [8, 9]. Rejection therefore means more than “VIX is persistent”: it means that the observed driver carries coupling structure beyond its own autocorrelation profile.

This placebo design is deliberately conservative. It does not test against white noise or against an unrelated macro covariate, both of which would be easy nulls. Instead it tests against fields with essentially the same low-order temporal persistence as the real series, which is the relevant adversarial explanation for any claim about inherited persistence [4, 8]. The empirical p -value is the fraction of placebo gains that equal or exceed the real ΔBIC improvement. Because only 100 placebos are used, the resolution is coarse, but the observed gap is so large that this discreteness is immaterial for the paper’s conclusions. The full placebo protocol is written out in Appendix B 1.

E. Directional diagnostics and mechanical versus informational overlap

Directionality is evaluated with manual bivariate Granger systems in both levels and first differences. The level test checks whether lagged VIX terms improve prediction of ψ_1 and vice versa. The differenced test is reported because near-integration can distort standard causality inference when persistent series are used in levels [48]. These Granger results are not treated as the primary identification device because rolling-window overlap and mild misspecification can still affect them, but they provide a useful directional sanity check alongside the placebo gate [9, 48].

Mechanical overlap is estimated by constructing a VIX proxy that preserves the empirical correlation path while suppressing time variation in per-stock volatilities. Concretely, for each stock i we compute its 60-day rolling volatility series, take the median of that series over the aligned sample, replace the time-varying volatility by that stock-specific median, and recompute an equal-weight portfolio variance using the actual rolling correlation matrices. The square root of that portfolio variance, after a single multiplicative rescaling to match the unconditional VIX level, defines the mechanical volatility proxy. This construction is not intended to reproduce the full option-integral definition of VIX; it is a controlled decomposition designed to ask how much of the ψ_1 association survives after the common realized-covariance channel is stripped down to its correlation component [19–21].

The informational component is then defined as the regression residual of actual $\log(\text{VIX})$ on the mechanical proxy. The mechanical and informational fractions reported in the Results section come from a sequential R^2 decomposition: first regress ψ_1 on the mechanical proxy alone, then add the informational residual and record the incremental gain. The same two components are also inserted separately into the M2 likelihood, producing

standalone field tests that directly assess whether model-selection power lives in the mechanical channel, the informational channel, or both. The static variance split is operational rather than unique, so we also repeat the construction under alternative volatility-freezing choices and portfolio weights. The point of those variants is not to force one canonical mechanical/informational percentage, but to test whether the sign and magnitude of the standalone field gains are recipe dependent [9, 19]. The exact algebra used for this decomposition is written out in Appendix A, and the full execution protocol is given in Appendix B 2.

F. Model-free persistence controls, non-overlapping reconstructions, and out-of-sample evaluation

The main one-dimensional claim is intentionally checked with controls that do not depend on the OU likelihood. The first is a quiet-regime autocorrelation comparison. Our strict ex ante criterion is daily VIX confined to [15, 18] for at least 120 consecutive trading days. Because that criterion yields no qualifying segment in 2004–2023, we adopt a transparent fallback based on a 20-day rolling-median VIX in [14, 20] and then repeat the calculation on neighboring bands [13, 21] and [15, 19]. For each accepted set of quiet segments, the autocorrelation function of ψ_1 is pooled across segments and summarized by the e-folding lag, defined as the first lag at which the ACF falls below e^{-1} of its lag-zero value. This diagnostic asks whether persistence collapses when the field is approximately quiescent, without assuming any specific stochastic model.

The second model-free control is the field-stripped residual

$$\epsilon_{\text{M2}}(t) = \psi_1(t) - \mu_{\text{eff}}(v_t), \quad (10)$$

where $\mu_{\text{eff}}(v_t) = \mu + (\beta/\theta)v_t$ is the fitted conditional equilibrium of M2. The ACF of ϵ_{M2} is compared with the ACF of raw ψ_1 through both e-folding lags and integrated ACF mass over fixed horizons. This control differs conceptually from the OU timescale ratio. The timescale ratio asks how fast the model relaxes conditional on the field; the residual ACF asks how much temporal structure remains after subtracting the fitted equilibrium path. The distinction is important enough that the comparison is revisited explicitly in the Discussion section. Full execution details for these controls are given in Appendix B 3.

A deeper measurement concern is overlapping windows. We therefore rebuild the one-dimensional comparison on disjoint weekly observables using 5-trading-day correlation windows sampled every 5 trading days, once for a weekly ψ_1 proxy and once for weekly mean market correlation. To probe the same-horizon extreme, we also construct disjoint 60-day block versions of ψ_1 and pair each block with either its end-of-block VIX value or its within-block mean VIX [38, 40]. These series are

lower power than the daily baseline, but they directly test whether the field-coupled model remains preferred once overlap is reduced or removed at the observable-construction stage. Their full execution details are also given in Appendix B 4.

Out-of-sample stability is assessed at two levels. The baseline split remains 2016-01-01: parameters are estimated on the pre-2016 observations and evaluated on the post-2016 observations under the same exact one-step Gaussian likelihood. Beyond that baseline, we run an anchored split sweep at 2010-01-01, 2012-01-01, 2014-01-01, 2016-01-01, 2018-01-01, and 2020-01-01, each time refitting on the available prefix and evaluating on the full remaining suffix. Performance is summarized by average log likelihood per observation, the test/train ratio, and the test-set likelihood gap between M2 and M0. This remains a chronological rather than cross-validated design, but it prevents the stability claim from hinging on a single historical partition [9]. The chronological holdout and anchored-sweep protocols are given in Appendix B 4.

G. Window-size robustness and resolution dependence

The window-robustness experiment is designed to answer a specific attack: whether the baseline conditioned timescale near 61 trading days is merely a restatement of the 60-day correlation window. We therefore recompute ψ_1 directly from raw returns for $W = 30, 45, 60, 90, 120$, refit M0 and M2 at each window, and record four quantities for every W : the bare timescale $\tau_0 = 1/\theta_0$, the conditioned timescale $\tau_{\text{cond}} = 1/\theta$, the susceptibility β/θ , and the scalar persistence-collapse attribution

$$\text{SCPA}(W) = 1 - \frac{\tau_{\text{cond}}(W)}{\tau_0(W)}. \quad (11)$$

The point of this sweep is not to demand that absolute timescales be identical across resolutions. Rolling correlation estimation is itself a low-pass filter, so absolute timescales can change mechanically with W . The relevant structural question is instead whether the field effect—as summarized by the susceptibility and by the sign and magnitude of SCPA—survives across resolutions. The quantitative results of that sweep are reported in Appendix Table IV, and the full execution protocol is given in Appendix B 4.

H. Exact two-dimensional extension and Wand-faithful weekly reconstruction

To test whether the observed VIX can itself play the role of the hidden variable behind apparent one-dimensional memory, we fit the exact linear-Gaussian

system

$$d\psi_1 = [-\theta_\psi(\psi_1 - \mu_\psi) + \beta_\psi v] dt + \sigma_\psi dW_1, \quad (12)$$

$$dv = [-\theta_v(v - \mu_v) + \beta_v \psi_1] dt + \sigma_v dW_2, \quad (13)$$

with $v = \log(\text{VIX})$ and correlated innovations. In discrete time this is an exact VAR(1) transition model whose restriction pattern determines whether the drift is decoupled, feedforward, or bidirectional [4, 6]. The fitted discrete transition matrix is mapped back to continuous time by matrix logarithm, and the innovation covariance is matched through the discrete Lyapunov equation, yielding exact continuous-time parameters within the linear-Gaussian class. The projected-memory derivation associated with this system is given in Appendix A.

The daily comparison alone is not enough because overlapping 60-day rolling windows can accentuate serial dependence. To compare more fairly with Wand *et al.*, we therefore reconstruct disjoint weekly observables using 5-trading-day correlation windows sampled every 5 trading days [38, 40]. This reconstruction is performed twice: once for a weekly ψ_1 proxy computed from each disjoint weekly matrix, and once for the mean market correlation of the same matrices. Both weekly series are passed through the same exact two-dimensional model comparison and projected-kernel calculations. This design keeps the hidden-variable test close to the preprocessing assumptions of the generalized-Langevin literature while preserving direct comparability with the daily model family. Full execution details for the 2D comparison are given in Appendix B 5.

I. Orthogonal residual state variable

The final construction is a level-orthogonal residual beyond the fitted conditional equilibrium. We estimate

$$\epsilon_\perp(t) = \psi_1(t) - [a + b \log(\text{VIX}(t))], \quad (14)$$

using ordinary least squares on levels, so that ϵ_\perp is approximately uncorrelated with $\log(\text{VIX})$ by construction. This object is not the same as ϵ_{M2} . The latter strips the fitted M2 equilibrium and is useful for persistence attribution; the former strips only the best linear level relation and is useful for asking whether an additional VIX-orthogonal state variable carries descriptive or predictive structure. We then partition the $(\log \text{VIX}, \epsilon_\perp)$ plane by the sample median of $\log \text{VIX}$ and by the sign of ϵ_\perp , producing the four quadrants used in the final results section.

The proposed predictive test compares future VIX changes after Q2 days (low VIX, positive ϵ_\perp) against Q3 days (low VIX, negative ϵ_\perp). We report mean future changes, Mann–Whitney p -values, and rank-biserial effect sizes at 30-, 60-, and 90-trading-day horizons. This is intentionally a narrow operational claim. A residual can be dynamically nontrivial without qualifying as a forecasting signal, and the analysis is designed to keep those two propositions separate [9, 44].

III. RESULTS

A. Empirical target

The quantity to explain is not merely the existence of crisis episodes with elevated collective correlation, but the fact that the full-sample autocorrelation of ψ_1 remains elevated for months. Figure 1 shows that ψ_1 co-moves strongly with VIX across the 2004–2023 sample while still exhibiting appreciable residual scatter around the observed volatility field proxy. The question throughout is whether this slow-looking behavior is intrinsic to ψ_1 or inherited from the motion of that observed proxy.

B. Conditional field-proxy decomposition

The one-dimensional stochastic hierarchy yields the clearest result of the paper. Table II summarizes the main model comparison. The main reference model remains the VIX-coupled Ornstein–Uhlenbeck model [5, 6, 21],

$$d\psi_1 = [-\theta(\psi_1 - \mu) + \beta \log(\text{VIX})] dt + \sigma dW, \quad (15)$$

with best-fit parameters $\theta = 0.01640$, $\mu = -0.6256$, $\beta = 0.00572$, and $\sigma = 0.00942$. The associated effective equilibrium is

$$\mu_{\text{eff}}(\text{VIX}) = \mu + \frac{\beta}{\theta} \log(\text{VIX}), \quad (16)$$

which evaluates numerically to $\mu_{\text{eff}}(\text{VIX}) = -0.626 + 0.349 \log(\text{VIX})$ on the aligned sample. This linear approximation is intended only over the observed VIX range of roughly 10–80. Extrapolation far below that range would imply unphysical negative equilibria once VIX falls below about 6, which simply reflects the local nature of the linearization.

At the baseline 60-day correlation-window construction, two timescales separate sharply. In the bare OU model, $\theta_0 = 0.00335$, giving an apparent relaxation time of roughly 298 trading days. In the VIX-coupled OU model, the intrinsic relaxation time conditional on the observed VIX proxy is roughly 61 trading days. The ratio $298/61 \approx 4.9$ means that, in OU-rate terms, conditioning on the observed VIX proxy removes about 79.5% of the apparent persistence. These timescales should be understood as model-implied relaxation rates under the fitted linear OU approximation, consistent with the pseudo-true interpretation adopted throughout.

The global BIC winner is the hybrid constrained regime-switching plus VIX model. Its fitted parameters, however, make its role quite specific: the calm state carries 98.7% of the stationary probability, the stress state lasts only about 1.1 trading days on average, and the continuous VIX loading remains large ($\beta = 0.00781$). In other words, the hybrid model is best read as a rare

TABLE II. Core one-dimensional and hybrid stochastic models on the aligned daily sample.

Model	BIC	$\Delta\text{BIC vs M2}$
M_RS,c+VIX	-33011.9	-765.4
M_RS,c	-32274.4	-27.9
M2'	-32255.3	-8.7
M2	-32246.5	0.0
M3	-32230.0	+16.5
M0	-32137.5	+109.0
M1	-32121.5	+125.0

extreme-event channel layered on top of the same continuous field effect isolated by M2 [46, 47]. The nested likelihood-ratio test against the regime-switching baseline is also decisive ($\chi^2 = 746$, $p \approx 0$), so the hybrid fit validates the coexistence of discrete extremes and continuous field motion rather than replacing the M2 interpretation [9, 46]. Within the hybrid model, the calm-state parameters imply an intrinsic timescale of roughly 43 trading days. The corresponding timescale ratio is therefore $1 - 43/298 \approx 0.86$, slightly above the M2-based estimate of 0.80. The qualitative conclusion is unchanged: most apparent persistence is field-inherited under either the M2 lens or the BIC-winning hybrid model. Complete parameter estimates for M_RS,c+VIX are reported in Appendix Table X.

Two negative results are equally central. A quartic model without an explicit field is strongly disfavored relative to the VIX-coupled OU model, and adding quartic structure on top of VIX does not improve the fit. Within the tested model family, the collective dynamics do not support a double-well or Ising-like interpretation [23, 28, 29].

The state-dependent-noise variant M2' provides only a modest refinement. Allowing $\sigma(\psi_1) = \sigma_0 + \sigma_1\psi_1$ improves BIC by 8.7 units relative to M2, indicating some structured heteroskedasticity, but it does not improve the most difficult high-VIX PIT diagnostic. We therefore retain the constant- σ M2 model as the primary interpretive lens and read M2' as a secondary adequacy check rather than as a change in the central attribution story [6, 9].

C. Placebo falsification and robustness controls

The strongest single discrimination test is the placebo-field experiment [8]. We generate 100 AR(9)-matched synthetic fields that reproduce the first-order persistence structure of $\log(\text{VIX})$ and compare their improvements against the real VIX field. None of the 100 surrogates matches the real VIX gain. The resulting distribution has mean $\Delta\text{BIC} = -6.5$, standard deviation 2.19, and maximum 2.70, versus 109.0 for the real VIX field. This excludes an explanation based on autocorrelation matching alone [8, 9].

Directionality supports the same picture. In the level-

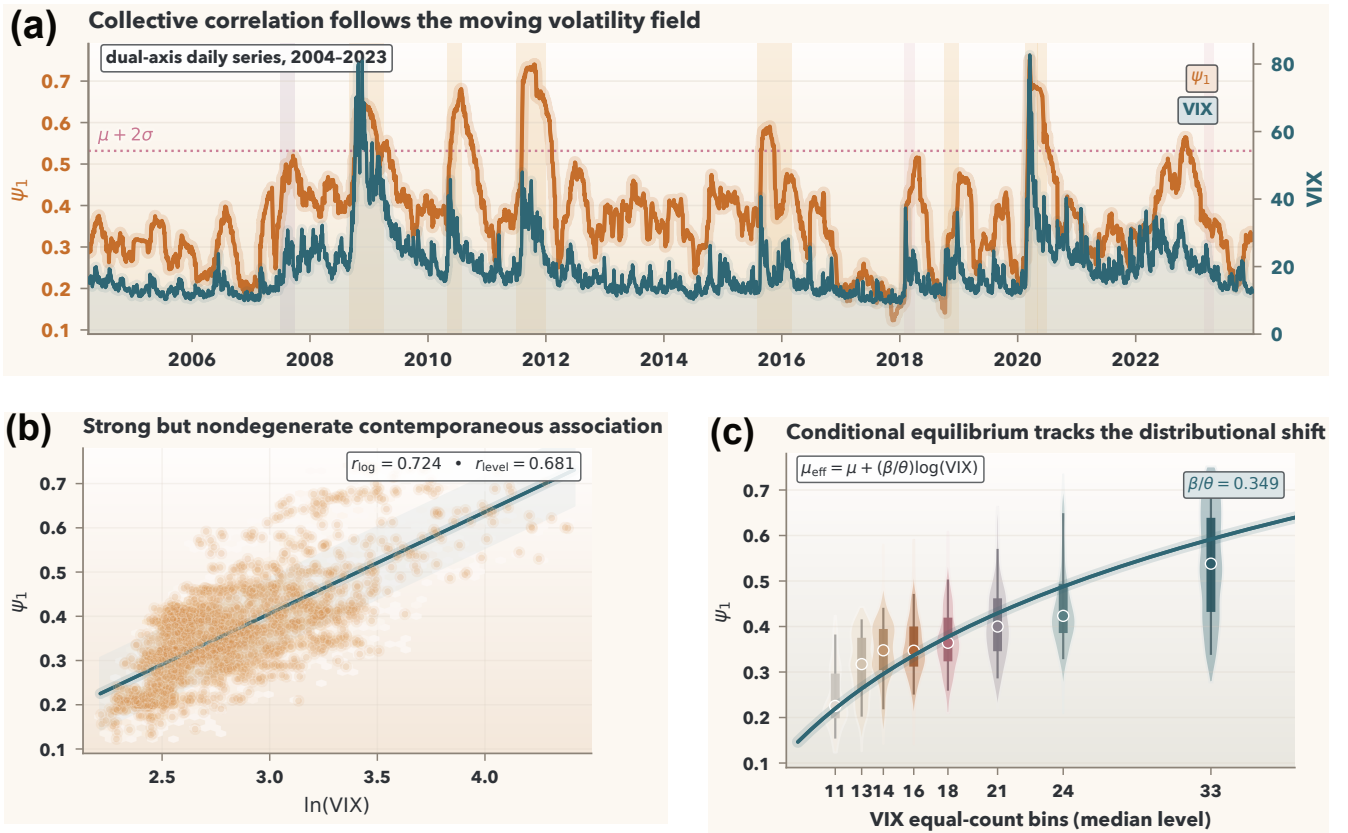


FIG. 1. **Collective correlation tracks a moving volatility field.** (a) The long-run ψ_1 series co-moves strongly with VIX over 2004–2023, with the largest excursions concentrated in major crisis episodes. (b) The contemporaneous association is strong but nondegenerate, with $r = 0.724$ against $\log(\text{VIX})$ and $r = 0.681$ against level VIX. (c) Equal-count VIX bins show that the fitted conditional equilibrium $\mu_{\text{eff}}(\text{VIX}) = \mu + (\beta/\theta)\log(\text{VIX})$ tracks the empirical shift of the ψ_1 distribution across volatility conditions. Together these panels motivate the attribution problem addressed below.

based Granger system, $\text{VIX} \rightarrow \psi_1$ dominates with $F = 15.07$ at lag 7, while the reverse direction is not significant in levels. Under first differencing, VIX still dominates ($F = 10.63$ versus 2.76), so the directional asymmetry is not a simple rolling-window overlap artifact [48].

The endogeneity objection is nevertheless real [19, 21]. Using the actual rolling correlation structure together with fixed median stock volatilities, we estimate that roughly 77.3% of the shared explanatory power in the $\text{VIX}-\psi_1$ relationship is mechanical and 22.7% is informational, with a partial residual correlation of about 0.60. Thus VIX is not a clean exogenous proxy in the strict physical sense. But the informational increment is substantial, and the placebo failure shows that it is not replaceable by generic persistence.

The strongest new evidence comes from fitting these two components as standalone fields. On the restricted sample where the split is defined, an M2 fit using the informational residual of $\log(\text{VIX})$ alone still improves on the bare OU benchmark by $\Delta\text{BIC} = 78.6$, whereas the mechanical proxy alone does not improve on the benchmark at all ($\Delta\text{BIC} = -8.3$). The full VIX field on that same restricted sample yields $\Delta\text{BIC} = 108.6$ (Appendix

Table V). In other words, the part of VIX that carries model-selection power is overwhelmingly informational rather than mechanical. The component gains are not expected to add up exactly, since the OU parameters are re-estimated for each effective field, but the dynamic implication is unambiguous: the main field-proxy attribution is not being generated by trivial overlap between realized volatility and realized correlation [9, 19].

That dynamic conclusion is not tied to a single decomposition recipe. Across three volatility-freezing choices (full-sample median, full-sample mean, and pre-2016 median) and three weighting schemes (equal, inverse-volatility, and volatility-share), the static mechanical fraction moves from 72.1% to 81.5% while the informational fraction moves from 18.5% to 27.9% (Appendix Table VI). But the dynamic result is invariant: informational-only fields remain strongly positive with ΔBIC in the narrow range 77.7–79.6, whereas mechanical-only fields remain BIC-negative in every tested variant ($-8.38 \leq \Delta\text{BIC} \leq -8.27$). The static split is therefore operational rather than unique, while the dynamic conclusion is highly stable across reasonable constructions [9, 19].

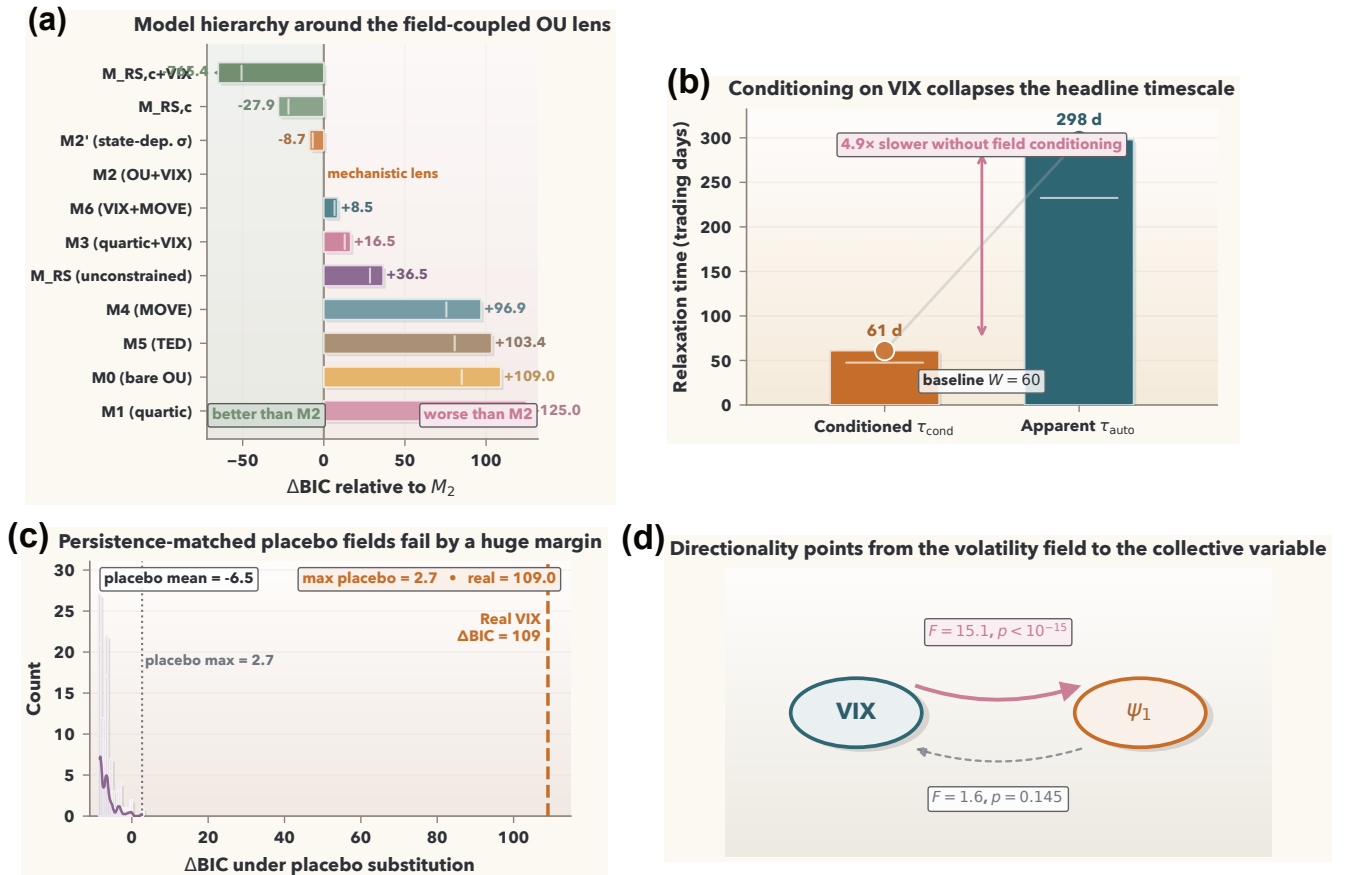


FIG. 2. **The main attribution result.** (a) Same-sample model comparison across the core, hybrid, and auxiliary-field variants centers the main interpretive story on the VIX-coupled OU model: bare OU and quartic alternatives are strongly disfavored, while rare-event hybrids are better read as an added extreme-state channel than as a replacement for the continuous field picture. (b) Under the baseline $W = 60$ construction, conditioning on VIX reduces the relaxation time from 298 to 61 trading days. (c) One hundred AR-matched placebo fields fail to approach the real-VIX gain (maximum placebo $\Delta\text{BIC} = 2.7$ versus 109 for real VIX). (d) Level-based Granger tests show dominant VIX \rightarrow ψ_1 directionality ($F = 15.1$ versus 1.6 in the reverse direction). These panels together establish the conditional field-proxy attribution that anchors the rest of the manuscript.

The overlapping-window concern can also be brought directly to the core one-dimensional claim. Rebuilding the observable from disjoint 5-trading-day correlation matrices sampled every 5 trading days, the field-coupled OU still beats bare mean reversion by $\Delta\text{BIC} = 151.2$ for weekly ψ_1 and by $\Delta\text{BIC} = 140.1$ for weekly mean market correlation (Appendix Table VII). On those disjoint weekly series the effective timescales shorten, as expected from the coarser clock, but the sign of the attribution result is unchanged: SCPA remains positive at 0.286 and 0.282, respectively. At the opposite extreme, a same-horizon disjoint 60-day block reconstruction yields only $\Delta\text{BIC} = 1.7$ when paired with end-of-block VIX and $\Delta\text{BIC} = -3.4$ when paired with block-mean VIX. We therefore interpret that 60-day block version as a low-power boundary check with only 77 observations, not as a power-matched replacement for the daily series. The main point is narrower but decisive: once overlap is removed in a reasonably information-preserving weekly re-

construction, the field-coupled model remains strongly preferred [9, 38, 40].

Cross-market auxiliary fields are weaker. MOVE provides only a modest same-sample gain ($\Delta\text{BIC} = 12.0$ versus the bare model), while TED does not improve the fit ($\Delta\text{BIC} = -1.1$). Several reasonable transformations of MOVE yield the same conclusion: it is auxiliary, not decisive. The strongest cross-field statement the current evidence supports is therefore modest: VIX is the uniquely strong field proxy in this dataset, MOVE is secondary, and TED does not help.

The stochastic fits are complemented by two model-free controls. The first is a quiet-regime autocorrelation check. The physically motivated strict criterion—daily VIX inside [15, 18] for at least 120 consecutive trading days—yields no qualifying segment in the entire sample. That absence is itself informative: the volatility field is never truly dormant for long, consistent with continual modulation of ψ_1 [1, 21]. To obtain a finite-sample

quiet-regime estimate, we therefore adopt a transparent relaxed criterion based on a 20-day rolling-median VIX in [14, 20], which yields three qualifying segments. Under that definition the e-folding lag drops from 69 days to 27 days, with an episode-bootstrap 95% confidence interval of [18, 33] days, the ACF at lag 20 falls from 0.853 to 0.514, and by lag 40 the quiet-regime ACF has already crossed below zero. The same 27-day e-folding lag is recovered under the wider [13, 21] band, whereas the narrower [15, 19] band yields no qualifying 120-day segment at all (Appendix Table IX). The quiet-regime diagnostic is therefore partially robust: it is replicated across the two widest tested bands, but finite-sample support disappears at the narrowest band.

The second control is a field-stripped residual. Defining

$$\epsilon_{M2}(t) = \psi_1(t) - \mu_{\text{eff}}(\text{VIX}(t)), \quad (17)$$

we find that the residual remains persistent, but much less so than raw ψ_1 : the e-folding lag drops from 69 to 42 days, the integrated ACF up to lag 60 drops from 44.3 to 30.6, and the integrated ACF up to lag 90 drops from 54.2 to 38.7. Field stripping therefore does not annihilate all persistence, but it removes a substantial fraction of it.

These controls are supported by a broader out-of-sample check. The baseline split at 2016-01-01 leaves the per-observation log likelihood of M2 almost unchanged between train and test periods (3.252 versus 3.235, ratio 0.995), which argues against the main result being a crisis-specific in-sample artifact. Because the post-2016 holdout contains the COVID-19 spike, we also repeat the evaluation after excluding 2020-03-01 through 2020-09-30 and scoring the two remaining contiguous test segments separately. The test log likelihood per observation then rises to 3.310, with a test/train ratio of 1.018, so the stability claim does not depend on the COVID episode. More importantly, a six-way anchored split sweep at 2010, 2012, 2014, 2016, 2018, and 2020 leaves the sign of the result unchanged on every held-out remainder: M2 beats M0 on test in all six cases, with per-observation test-set gains ranging from 0.0023 to 0.0152 and M2 test/train ratios ranging from 0.964 to 0.999 (Appendix Table VIII). The field-coupled advantage is therefore not tied to a single historical partition [9].

An exact raw-return window sweep sharpens the interpretation of the headline timescale. Recomputing ψ_1 directly from returns for $W = 30, 45, 60, 90, 120$ leaves the field advantage intact at every window ($\Delta\text{BIC} = 99\text{--}165$ for M2 over M0) and keeps the field susceptibility β/θ in a narrow range of 0.336–0.376 (Appendix Table IV). The absolute conditioned timescale is not window-invariant: it rises from 34 trading days at $W = 30$ to 97 trading days at $W = 120$, while the bare timescale rises from 105 to 839 days. This behavior is expected from the low-pass filtering inherent in rolling-window estimation. The more structural quantity is the susceptibility β/θ , which determines the equilibrium displacement per unit of $\log(\text{VIX})$ and remains stable across all tested windows. The at-

tribution fraction itself, measured by $1 - \tau_{\text{cond}}/\tau_{\text{auto}}$, remains majority-inherited at every window but increases from 0.67 to 0.88 rather than staying strictly constant. The 61-day figure should therefore be read as the effective conditioned timescale at the baseline resolution $W = 60$, not as a window-independent physical constant [6, 9]. The monotonic increase of SCPA with W is itself consistent with rolling-window low-pass filtering, which inflates the bare timescale more strongly because the bare model must absorb field-driven slow motion that the conditioned model removes explicitly. The formal limit $W \rightarrow 0$ is not an operational object for rolling-correlation estimation: while the leading eigenvalue fraction remains estimable in the high-dimensional $W < N$ regime, arbitrarily short windows would collapse the statistic into finite-sample noise [14]. The smallest analyzed window here is $W = 30$, where the bare timescale is still 105 trading days, already well above the window length itself.

D. Two-dimensional hidden-variable extension

The strongest theoretical extension was to ask whether the observed VIX can itself serve as the hidden variable behind one-dimensional generalized Langevin memory [4, 38, 40]. The following extension is exact only within the linear-Gaussian class, with nonlinear departures treated as a limitation rather than silently absorbed into the interpretation [6, 9]. To test this, we fit an exact linear-Gaussian two-dimensional system,

$$d\psi_1 = [-\theta_\psi(\psi_1 - \mu_\psi) + \beta_\psi v] dt + \sigma_\psi dW_1, \quad (18)$$

$$dv = [-\theta_v(v - \mu_v) + \beta_v \psi_1] dt + \sigma_v dW_2, \quad (19)$$

with $v = \log(\text{VIX})$ and correlated innovations. Because the one-step transition density is exactly Gaussian, the discrete VAR(1) likelihood is the exact transition-density MLE within this model family.

On the aligned daily series, feedforward coupling is preferred over bidirectional drift by $\Delta\text{BIC} = 2.4$, while the feedforward model beats the decoupled model by $\Delta\text{BIC} = 125.3$. The $\Delta\text{BIC} = 2.4$ margin between feedforward and bidirectional drift is small by conventional model-selection standards [10], so the daily data offer only a weak preference for the simpler feedforward form. The preferred daily model reproduces the one-dimensional M2 parameters on the ψ_1 side almost exactly, but sets $\beta_v = 0$ in the best structure. On the daily sample, observed VIX behaves as a persistent driver, not as a preferred hidden variable whose elimination generates a self-memory kernel [4, 38].

The key stress test is therefore the Wand-faithful weekly construction. The daily series is built from overlapping windows, which can accentuate serial dependence and may sharpen the appearance of one-way drive. We therefore rebuild the problem using disjoint 5-day correlation windows sampled every 5 trading days, much closer to the preprocessing in the generalized-Langevin

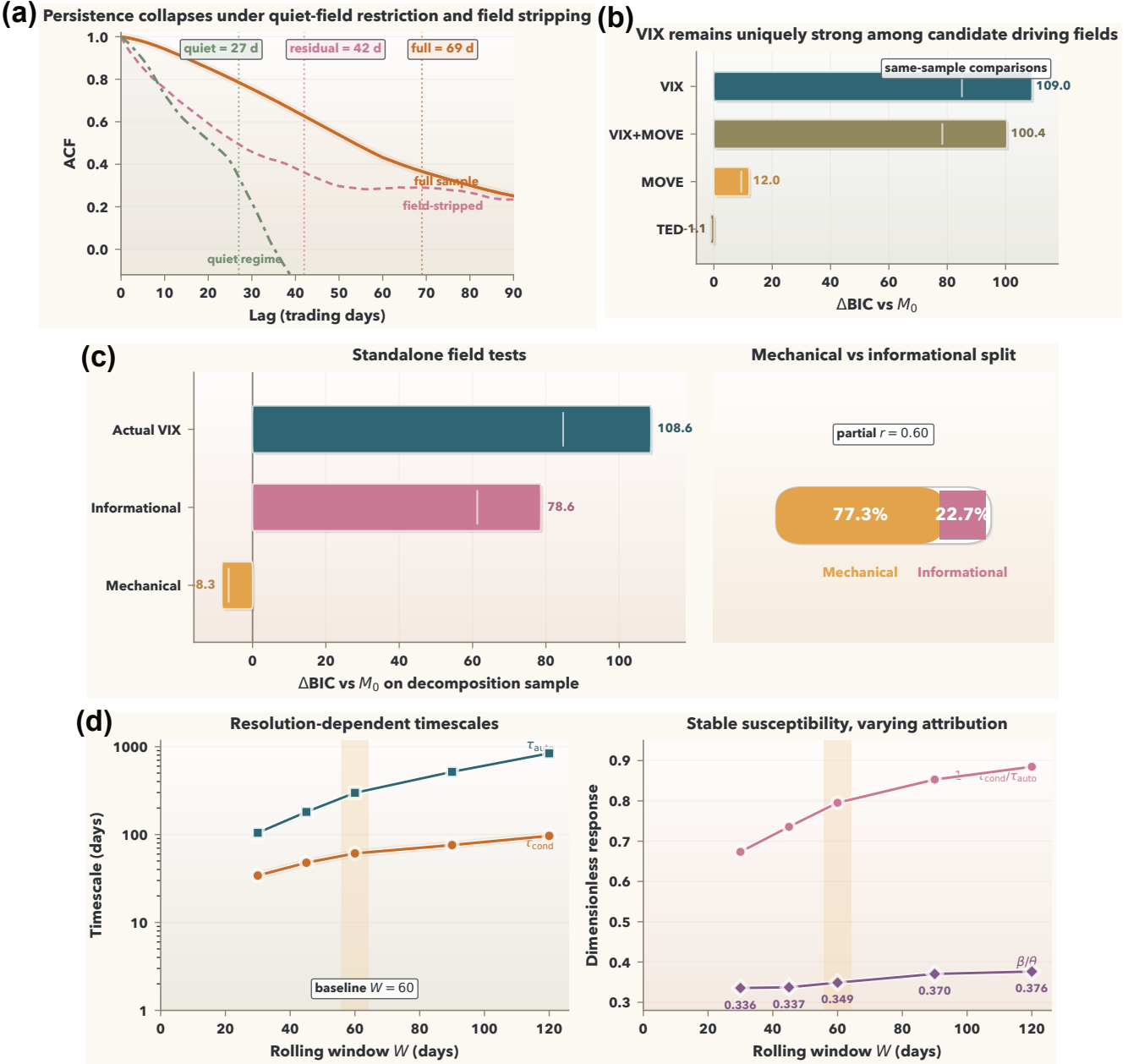


FIG. 3. **Independent robustness checks.** (a) Persistence collapses both in quiet regimes and after subtracting the fitted VIX-dependent equilibrium: the full-sample e-folding lag is 69 trading days, the field-stripped residual falls to 42 days, and the quiet-regime estimate falls to 27 days. (b) Among auxiliary fields, VIX remains uniquely strong, while MOVE is secondary and TED does not improve on the bare benchmark. (c) On the decomposition sample, the informational residual of $\log(\text{VIX})$ alone retains most of the model-selection gain ($\Delta\text{BIC} = 78.6$), whereas the mechanical proxy alone fails to improve the fit ($\Delta\text{BIC} = -8.3$); the same sample still yields a 77.3%/22.7% mechanical/informational variance split. (d) Exact recomputation across $W = 30\text{--}120$ shows that absolute timescales depend on rolling-window resolution, but the field susceptibility β/θ stays in the narrow range 0.336–0.376 and the attribution fraction remains majority-inherited at every window. Together these panels show that the main claim is not an artifact of placebo persistence, auxiliary fields, mechanical overlap, or the baseline window choice.

literature [38, 40]. Under this construction the evidence changes: a weekly ψ_1 proxy weakly prefers the full bidirectional model by $\Delta\text{BIC} = 0.78$ over feedforward, and the weekly mean market correlation weakly prefers it by $\Delta\text{BIC} = 2.69$.

This is the strongest surviving part of the hidden-

variable story: bidirectional structure becomes more plausible once the comparison is made under a preprocessing regime close to the prior weekly work. But the bridge still stops short of full identification [4, 7]. Solving the second equation formally and substituting into

the first yields a projected memory term of the form

$$K(t) = \beta_\psi \beta_v e^{-\theta_v t}, \quad (20)$$

plus colored-noise contributions. The implied timescales are not close to the conservative ~ 15 -day benchmark implied by “three trading weeks” in Wand *et al.* On our outputs they are approximately 36.5 days for the daily full model, 9.1 days for naive weekly thinning, 33.5 days for the Wand-faithful weekly ψ_1 proxy, and 36.5 days for the Wand-faithful mean market correlation. The bridge is therefore nontrivial but incomplete: a more faithful weekly comparison makes bidirectional coupling more plausible, yet observed VIX still does not recover the reported generalized-Langevin memory scale.

The 2D placebo gate still adds independent value. The daily feedforward model beats the daily decoupled model by roughly 125 BIC units, and none of 100 AR-matched placebo fields reproduces the real coupling gain. So the 2D section remains essential even though it supports only partial reconciliation rather than full unification.

E. Orthogonal residual analysis

The final analytical step asks whether a residual order parameter beyond VIX can carry operational information. Two residuals are useful to distinguish [9, 44]. The mechanistic residual,

$$\epsilon_{M2}(t) = \psi_1(t) - \mu_{\text{eff}}(\text{VIX}(t)), \quad (21)$$

is natural for field-stripping but not orthogonal to VIX in levels. The relevant candidate order parameter is instead the orthogonal level residual,

$$\epsilon_\perp(t) = \psi_1(t) - (a + b \log(\text{VIX}(t))), \quad (22)$$

where (a, b) are estimated from a direct level regression and therefore enforce $\text{corr}(\epsilon_\perp, \log \text{VIX}) \approx 0$.

This variable is not trivial noise. Its e-folding lag is about 43 days, compared with 69 days for raw ψ_1 , and its integrated ACF to lag 60 is 32.1 instead of 44.3. In that sense, ϵ_\perp is a genuine residual mode rather than a negligible leftover.

The associated phase-space program is only partially successful. Partitioning the $(\log \text{VIX}, \epsilon_\perp)$ plane by the sample median of $\log \text{VIX}$ and the sign of ϵ_\perp yields balanced time fractions overall, but event-peak classification is less rich than hoped: Q1 contains six peak events, Q4 contains three, Q2 contains only China/Oil 2015–16, and Q3 contains none of the predefined event peaks. Thus the phase space is descriptive, but not a mature four-state taxonomy.

The strongest proposed operational test also fails. Comparing low-VIX/high- ϵ_\perp (Q2) days against low-VIX/low- ϵ_\perp (Q3) days, we find no evidence that Q2 precedes larger future VIX increases at 30, 60, or 90 trading days. The mean differences are small, the Mann-Whitney tests are not significant, and the associated

TABLE III. Future VIX changes after low-VIX days split by the sign of the orthogonal residual. Positive rank-biserial values would favor the proposed Q2 signal.

Horizon	Mean Q2	Mean Q3	Mann-Whitney p	Rank-biserial
30 days	0.078	0.083	0.183	0.021
60 days	0.082	0.135	0.736	-0.015
90 days	0.110	0.141	0.986	-0.052

rank-biserial effect sizes remain close to zero (Table III). The orthogonal residual therefore survives as a descriptive state variable, but not as a demonstrated forecasting signal.

Taken together, the results define a deliberately uneven evidence profile: the conditional field-proxy decomposition is strongly supported, the two-dimensional bridge is only partially supported, and the orthogonal residual is descriptive rather than predictive.

IV. DISCUSSION

The central result is conditional rather than fully causal: within the tested stochastic class, most apparent persistence in market collective correlation is absorbed once one conditions on an observed VIX field proxy rather than leaving the dynamics bare. The strongest contribution of the paper is therefore not a universal hidden-variable model, but a falsifiable attribution protocol that sharply narrows the interpretation of slow collective dynamics [4, 8, 9]. A field-coupled OU model, a placebo gate that rejects autocorrelation-matched surrogates, disjoint weekly reconstructions that preserve the M2 advantage, decomposition variants that leave informational-only fields strongly positive while mechanical-only fields remain negative, and both quiet-regime and field-stripped ACF collapse all point in the same direction. This convergence is unusually strong for a soft-system inference problem [19, 20, 43, 49].

A. Reconciling persistence attribution measures

Two quantitative attribution measures appear in this paper and should not be conflated. The timescale ratio $1 - \tau_{\text{cond}}/\tau_{\text{auto}} \approx 0.80$ compares model-implied OU relaxation rates before and after conditioning on VIX [5, 6]. By contrast, the field-stripped residual ACF reduction of about 39% compares the e-folding lag of raw ψ_1 against that of $\epsilon_{M2} = \psi_1 - \mu_{\text{eff}}(\text{VIX})$, dropping from 69 to 42 trading days. The first quantity is a model-based rate comparison within the OU class; the second is a model-free comparison of the temporal structure left after subtracting the fitted conditional equilibrium.

These numbers need not agree. The timescale ratio measures how fast ψ_1 relaxes toward a moving VIX-dependent target once that target is specified. The resid-

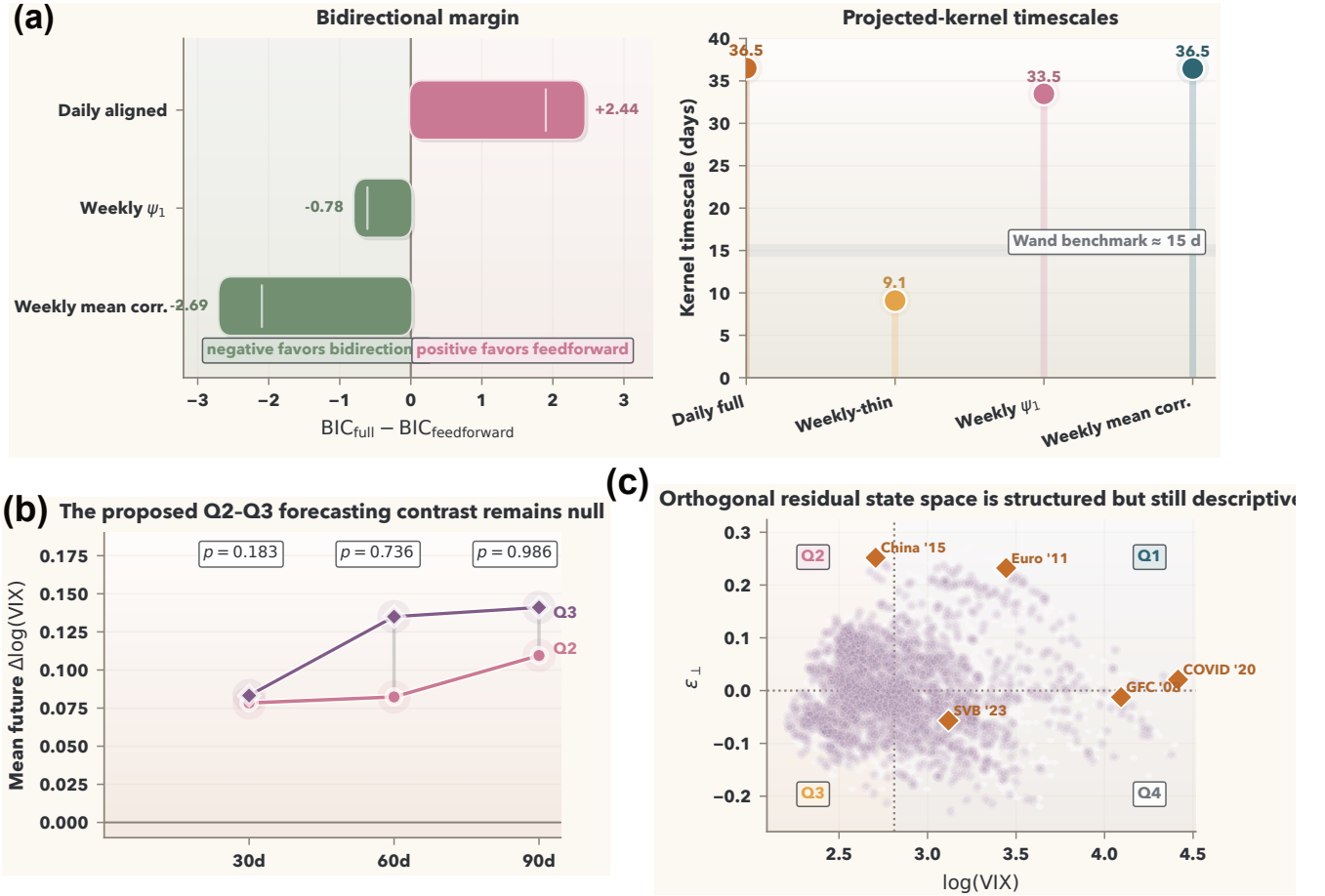


FIG. 4. **Extensions beyond the main one-dimensional result.** (a) On daily aligned data the 2D comparison weakly favors feedforward over bidirectional drift by $\Delta\text{BIC} = 2.44$, whereas the Wand-faithful weekly reconstructions weakly favor bidirectionality ($\Delta\text{BIC} = -0.78$ for weekly ψ_1 and -2.69 for weekly mean correlation; negative values favor bidirectional coupling). The projected-kernel timescales remain in the 9–36 day range and therefore do not recover the 15-day Wand benchmark in any clean way. (b) The orthogonal residual phase space in $(\log \text{VIX}, \epsilon_{\perp})$ is structured and visually nontrivial. (c) The proposed Q2-versus-Q3 prediction test nevertheless remains null across all tested horizons ($p = 0.183, 0.736, \text{ and } 0.986$ at 30, 60, and 90 trading days). The figure therefore frames these sections as constrained extensions rather than as new headline results.

ual ACF measures how much persistence remains after that target is subtracted, including persistence from imperfect linearization, additional latent drivers, and rolling-window measurement structure [6, 9]. They therefore bracket the field effect from different angles rather than estimating a single universal percentage.

A further caveat is that the absolute OU timescales are resolution-dependent. Exact recomputation with $W = 30\text{--}120$ shows that the conditioned relaxation time increases from 34 to 97 trading days as the rolling window lengthens, which is consistent with the low-pass filtering built into rolling-window observables [6, 9]. The more structural quantity is the susceptibility β/θ , which remains stable across those windows in the narrow range 0.336–0.376. By contrast, the model-based attribution fraction $1 - \tau_{\text{cond}}/\tau_{\text{auto}}$ is not strictly invariant: it stays in the majority-inherited regime for every window, but rises from about 0.67 to 0.88 as W increases. The baseline

61-day estimate should therefore be read as the effective conditioned timescale of the standard $W = 60$ construction, not as a window-free microscopic constant.

The two-dimensional extension refines that conclusion without overturning it. On the aligned daily sample, observed VIX behaves as a persistent driver and not as the preferred hidden coordinate whose projection would reproduce generalized-Langevin memory. At the same time, the Wand-faithful weekly reconstruction does revive weak bidirectional preference, though still within the inconclusive BIC range, so the relation to Wand *et al.* is more nuanced than simple contradiction. We also note that the Wand sample (1992–2012, $N = 249$) differs from ours in both period and stock universe, so part of the kernel-timescale discrepancy may reflect data differences rather than a fundamental failure of the Mori–Zwanzig identification. The most defensible synthesis is partial reconciliation: explicit field driving and hidden-

variable memory are not unrelated descriptions, but observed VIX alone does not complete the Mori–Zwanzig identification [4, 7, 38, 40].

The orthogonal residual extension leads to a parallel lesson. Constructing ϵ_{\perp} is easy, and its dynamics are not trivial. It yields a genuine VIX-orthogonal residual mode with intermediate persistence and some event-classification structure. But that is not the same as demonstrating an operationally useful predictive order parameter [9]. The negative Q2-versus-Q3 tests show why it is worth keeping those claims separate. This residual also differs conceptually from the implied-correlation versus realized-correlation gaps studied in the correlation-risk-premium literature [44]: here the object is an orthogonalized collective state variable, not an option-pricing spread.

These results sharpen the relation to the criticality literature. The present evidence does not support a double-well, Ising-like, or critical-slowness interpretation of ψ_1 dynamics [1, 23–27]. Within the tested stochastic class, the physical picture is closer to a driven single-well system with persistent field motion and a modest complementary extreme-state channel [5, 6]. Strong visual persistence of the collective variable is therefore not, by itself, evidence for a near-critical endogenous transition [1, 9].

This also clarifies the relation to earlier Kramers–Moyal extractions for financial correlation observables. Unlike Stepanov *et al.*, who extracted Kramers–Moyal coefficients for a related dominating correlation variable without testing external fields explicitly, the present work conditions on candidate drivers and subjects them to placebo-surrogate discrimination [8, 42].

More broadly, the methodology should transfer to other soft complex systems. Dynamic functional connectivity in fMRI or EEG, delayed climate indices, and ecological synchrony measures all face the same question: is the slow observable intrinsically slow, or is it being dragged by a persistent field proxy [1, 2, 7]? The same placebo-controlled sequence used here can be applied there as well: compare bare and field-coupled stochastic models, reject persistence-only surrogates, quantify mechanical overlap where needed, and only then test stronger hidden-variable or residual-state interpretations [4, 7, 8]. Exact multivariate OU fits also open a route to nonequilibrium diagnostics such as entropy-production measures [45].

Abstracted away from finance, the protocol has four generic ingredients: a collective observable, an observed candidate field proxy on the same clock, a field-free versus field-coupled stochastic comparison with matched likelihood treatment, and an adversarial surrogate or decomposition stage that attacks persistence-only and mechanical-only explanations [4, 8, 9]. It is strongest when the observable can be reconstructed at multiple resolutions and when a non-overlapping version is available. Its generic failure mode is latent common drive: if an unobserved z moves both the proxy and the observable, the protocol can still show that conditioning on the proxy re-

moves apparent persistence, but it cannot by itself prove direct coupling from proxy to observable [4, 7, 9].

B. Limitations

Several limits remain important. First, the VIX relationship is materially mechanical even after the decomposition [19, 21]. The static mechanical share is operational rather than unique: across reasonable freeze and weighting schemes it ranges from 0.72 to 0.81, even though the dynamic model-selection conclusion remains invariant. Second, MOVE and TED do not support a broader cross-market hierarchy beyond the main VIX result. Third, the two-dimensional extension is exact only within a linear-Gaussian class, and the state-dependent-noise diagnostics indicate structured inadequacies in extreme regimes [6, 9]. Fourth, the event sample is still small relative to the breadth of financial stress phenomenology. Finally, the main failure mode of the attribution protocol is a latent common driver that is only imperfectly proxied by the observed field proxy; placebo rejection against the observed proxy does not eliminate that possibility [4, 9]. More precisely, the placebo gate tests whether the observed proxy carries coupling information beyond marginal persistence, but it does not by itself distinguish direct coupling $u \rightarrow y$ from a confounded structure in which an unobserved driver z influences both the proxy u and the observable y .

These caveats define the paper’s boundary rather than its weakness. The manuscript is strongest on conditional field-proxy attribution, more limited on the hidden-variable bridge, and explicitly negative on operational residual prediction. These boundaries delineate what can and cannot be concluded from the present evidence.

DATA AVAILABILITY

Daily VIX closes were obtained from Federal Reserve Economic Data. The processed datasets needed to reproduce the figures and tables in this manuscript are available from the authors on reasonable request.

CODE AVAILABILITY

The analysis and figure-generation code used for this manuscript are available from the authors on reasonable request.

Appendix A: Exact Likelihoods and Analytical Derivations

1. Exact one-dimensional transition laws

For the bare OU model,

$$d\psi_t = -\theta_0(\psi_t - \mu_0) dt + \sigma_0 dW_t, \quad (\text{A1})$$

the exact solution over one unit daily interval is

$$\psi_{t+1} = e^{-\theta_0} \psi_t + (1 - e^{-\theta_0}) \mu_0 + \eta_t, \quad (\text{A2})$$

with Gaussian innovation

$$\eta_t \sim \mathcal{N}(0, q_0), \quad (\text{A3})$$

$$q_0 = \frac{\sigma_0^2}{2\theta_0} (1 - e^{-2\theta_0}), \quad (\text{A4})$$

which is the standard exact transition density of the Ornstein–Uhlenbeck process [5, 6]. The one-step log likelihood is

$$\begin{aligned} \ell_{M0} &= -\frac{n-1}{2} \log(2\pi q_0) \\ &\quad - \frac{1}{2q_0} \sum_{t=1}^{n-1} (\psi_{t+1} - m_t^{(0)})^2, \end{aligned} \quad (\text{A5})$$

where $m_t^{(0)} = e^{-\theta_0} \psi_t + (1 - e^{-\theta_0}) \mu_0$.

For the field-coupled model,

$$d\psi_t = [-\theta(\psi_t - \mu) + \beta v_t] dt + \sigma dW_t, \quad (\text{A6})$$

we treat the observed field value $v_t = \log(\text{VIX}_t)$ as constant on the interval $[t, t+1)$. Variation of constants gives

$$\begin{aligned} \psi_{t+1} &= e^{-\theta} \psi_t \\ &\quad + \int_t^{t+1} e^{-\theta(t+1-s)} (\theta\mu + \beta v_t) ds + \int_t^{t+1} e^{-\theta(t+1-s)} \sigma dW_s. \end{aligned} \quad (\text{A7})$$

The deterministic integral evaluates to

$$(1 - e^{-\theta}) \left(\mu + \frac{\beta}{\theta} v_t \right), \quad (\text{A8})$$

and the stochastic integral is Gaussian with variance $\sigma^2(1 - e^{-2\theta})/(2\theta)$ [5, 6]. Hence

$$\psi_{t+1} | \psi_t, v_t \sim \mathcal{N}(m_t^{(2)}, q), \quad (\text{A9})$$

$$m_t^{(2)} = e^{-\theta} \psi_t + (1 - e^{-\theta}) \left(\mu + \frac{\beta}{\theta} v_t \right), \quad (\text{A10})$$

$$q = \frac{\sigma^2}{2\theta} (1 - e^{-2\theta}). \quad (\text{A11})$$

The corresponding log likelihood is

$$\begin{aligned} \ell_{M2} &= -\frac{n-1}{2} \log(2\pi q) \\ &\quad - \frac{1}{2q} \sum_{t=1}^{n-1} (\psi_{t+1} - m_t^{(2)})^2. \end{aligned} \quad (\text{A12})$$

The quantities reported in the main text are then

$$\tau_{\text{auto}} = \frac{1}{\theta_0}, \quad (\text{A13})$$

$$\tau_{\text{cond}} = \frac{1}{\theta}, \quad (\text{A14})$$

$$\chi = \frac{\beta}{\theta}, \quad (\text{A15})$$

$$\mu_{\text{eff}}(v) = \mu + \chi v, \quad (\text{A16})$$

where χ is the field susceptibility, i.e. the equilibrium displacement per unit of $\log(\text{VIX})$.

2. Mechanical and informational field decomposition

Let m_t denote the mechanical volatility proxy and $a_t = \log(\text{VIX}_t)$ denote the actual field. The informational residual is defined by the auxiliary regression

$$a_t = \gamma_0 + \gamma_1 m_t + r_t, \quad (\text{A17})$$

so that r_t is orthogonal to the fitted mechanical component in sample. We then fit the sequential regressions

$$\psi_t = \alpha_0 + \alpha_1 m_t + u_t, \quad (\text{A18})$$

$$\psi_t = \beta_0 + \beta_1 m_t + \beta_2 r_t + \varepsilon_t. \quad (\text{A19})$$

If R_{mech}^2 is the coefficient of determination of the first regression and R_{full}^2 that of the second, the reported fractions are

$$f_{\text{mech}} = \frac{R_{\text{mech}}^2}{R_{\text{full}}^2}, \quad (\text{A20})$$

$$f_{\text{info}} = \frac{R_{\text{full}}^2 - R_{\text{mech}}^2}{R_{\text{full}}^2}. \quad (\text{A21})$$

With the decomposition sample used in the manuscript, $R_{\text{full}}^2 = 0.7120$, $R_{\text{mech}}^2 = 0.5505$, and the informational increment is 0.1615, yielding $f_{\text{mech}} = 0.7732$ and $f_{\text{info}} = 0.2268$. These quantities summarize shared explanatory power in a static regression sense; they do not imply that the standalone OU-field improvements must add linearly, because the M2 parameters are re-estimated for each field and the fitted equilibrium map changes with the field definition [9]. That is precisely why the separate M2 fits with actual, mechanical-only, and informational-only fields are reported as distinct experiments rather than algebraically combined.

3. Two-dimensional OU projection and induced memory kernel

Write the centered two-dimensional system as

$$\dot{\mathbf{x}}(t) = \mathbf{A}\mathbf{x}(t) + \Sigma\xi(t), \quad (\text{A22})$$

$$\mathbf{x}(t) = \begin{pmatrix} \psi_1(t) - \mu_\psi \\ v(t) - \mu_v \end{pmatrix}, \quad (\text{A23})$$

with drift matrix

$$\mathbf{A} = \begin{pmatrix} -\theta_\psi & \beta_\psi \\ \beta_v & -\theta_v \end{pmatrix}. \quad (\text{A24})$$

The exact discrete transition over one interval Δ is

$$\mathbf{x}_{t+\Delta} = e^{\mathbf{A}\Delta}\mathbf{x}_t + \boldsymbol{\eta}_t, \quad (\text{A25})$$

$$\boldsymbol{\eta}_t \sim \mathcal{N}(0, Q_\Delta), \quad (\text{A26})$$

with covariance

$$Q_\Delta = \int_0^\Delta e^{As} \Sigma \Sigma^\top e^{A^\top s} ds, \quad (\text{A27})$$

which is the exact continuous-time/discrete-time correspondence for linear-Gaussian systems [4, 6]. The structural restrictions used in the paper are: decoupled ($\beta_\psi = \beta_v = 0$), feedforward ($\beta_\psi \neq 0, \beta_v = 0$), and bidirectional ($\beta_\psi \neq 0, \beta_v \neq 0$). The daily and weekly comparisons are carried out by exact Gaussian likelihood in this discrete representation, and the continuous-time coefficients are obtained by matrix logarithm of the estimated transition matrix.

To expose the projected-memory interpretation, solve the second equation formally:

$$v(t) = v(0)e^{-\theta_v t} + \int_0^t e^{-\theta_v(t-s)} [\beta_v \psi_1(s) ds + \sigma_v dW_2(s)]. \quad (\text{A28})$$

Substituting this expression into the observable equation yields

$$\begin{aligned} \dot{\psi}_1(t) &= -\theta_\psi \psi_1(t) + \beta_\psi v(0)e^{-\theta_v t} \\ &+ \beta_\psi \beta_v \int_0^t e^{-\theta_v(t-s)} \psi_1(s) ds \\ &+ \beta_\psi \sigma_v \int_0^t e^{-\theta_v(t-s)} dW_2(s) + \sigma_\psi \xi_1(t). \end{aligned} \quad (\text{A29})$$

The induced self-memory kernel is therefore

$$K(t) = \beta_\psi \beta_v e^{-\theta_v t}, \quad (\text{A30})$$

and the associated projected timescale is $\tau_K = 1/\theta_v$ [4, 7]. When $\beta_v = 0$, as in the daily-preferred feedforward structure, this kernel vanishes identically. The observed VIX can only generate a nonzero projected memory kernel when the bidirectional term is empirically supported.

4. Definitions of attribution measures

Two attribution measures are used repeatedly in the manuscript. The first is the model-based scalar persistence-collapse attribution

$$\text{SCPA} = 1 - \frac{\tau_{\text{cond}}}{\tau_{\text{auto}}} = 1 - \frac{\theta_0}{\theta}, \quad (\text{A31})$$

which compares OU timescales before and after field conditioning. The second is the model-free field-stripped persistence reduction, computed from the e-folding lag or integrated ACF of ψ_1 versus that of $\epsilon_{M2} = \psi_1 - \mu_{\text{eff}}(v)$. These measures are not expected to coincide exactly because they summarize different objects: one is a rate parameter inside the fitted OU class, while the other is a residual temporal statistic that remains sensitive to latent drivers, nonlinearity, and rolling-window measurement effects [6, 9]. The manuscript therefore interprets them jointly rather than forcing them into a single percentage.

Appendix B: Robustness Experiment Design and Execution

1. Placebo-field protocol

The placebo experiment is executed as a fixed pipeline rather than as an informal sensitivity check. First, we fit an AR(p) model to the aligned log(VIX) series, selecting p by AIC over $p = 1, \dots, 10$; this chooses $p = 9$ on the aligned sample. Second, we simulate 100 independent surrogate paths of the same length as the empirical field, using the fitted AR recursion and independent Gaussian innovations. Third, each path is linearly rescaled to the empirical mean and variance of the real log(VIX) series so that only the coupling information, not the marginal scale, can

differentiate the real and placebo fields. Fourth, each surrogate replaces the real field in the exact M2 likelihood, and the improvement over M0 is recorded as $\Delta\text{BIC}_{\text{placebo}}$. Fifth, the empirical p -value is computed as the fraction of placebo gains that meet or exceed the real gain [8, 9]. The same logic is reused in the 2D daily placebo gate, where feedforward and full bidirectional models are compared against the decoupled benchmark under persistence-matched placebo drivers.

2. Mechanical-proxy construction and standalone field tests

The mechanical proxy is constructed on the same aligned daily sample used for the main M2 fit. For each stock i , let $s_{i,t}$ denote the 60-day rolling volatility and let $\tilde{s}_i = \text{median}_t s_{i,t}$ be its sample median over the aligned period. With equal portfolio weights $w_i = 1/N$, the mechanical portfolio variance is

$$\widehat{V}_t^{\text{mech}} = \sum_{i=1}^N \sum_{j=1}^N w_i w_j \tilde{s}_i \tilde{s}_j C_{ij}(t). \quad (\text{B1})$$

The mechanical VIX proxy is then

$$\text{VIX}_{\text{mech},t} = c \sqrt{\widehat{V}_t^{\text{mech}}}, \quad (\text{B2})$$

where the scalar c is chosen so that the proxy matches the sample mean of the observed VIX. The informational component is defined by residualizing $\log(\text{VIX}_t)$ on $\log(\text{VIX}_{\text{mech},t})$. The design then branches into two complementary evaluations. A static regression decomposition yields the mechanical and informational fractions of shared explanatory power. Separate M2 fits using the actual field, the mechanical proxy, and the informational residual then ask which component carries standalone model-selection power. The key inference is dynamic rather than purely correlational: even if the mechanical proxy is highly correlated with ψ_1 , it does not count as explanatory unless it improves the stochastic likelihood over M0.

To test recipe sensitivity, we repeat the construction under three volatility-freezing statistics and three weighting schemes. The freeze variants are the full-sample median, the full-sample mean, and the pre-2016 median of each stock's 60-day rolling volatility. The weighting variants are equal weights, inverse-volatility weights, and volatility-share weights. Every variant is pushed through the same two outputs: the static regression decomposition and the standalone M2 fits with mechanical-only and informational-only fields. This keeps the sensitivity analysis aligned to the reviewer's actual concern, namely whether the qualitative model-selection conclusion changes under reasonable alternative constructions.

3. Quiet-regime pooling and field-stripped ACF evaluation

The quiet-regime experiment is executed in two passes. The strict pass scans the aligned daily sample for maximal contiguous segments in which the daily VIX level remains inside [15, 18] for at least 120 consecutive trading days. When that yields no valid segment, the fallback pass replaces the raw daily VIX by a 20-day rolling median and scans three neighboring bands: [13, 21], [14, 20], and [15, 19]. For each band, all maximal contiguous segments with length at least 120 trading days are retained. Within each segment we compute the sample ACF of ψ_1 , then pool the segment-specific ACFs by available pair counts at each lag. The e-folding lag is reported as the first lag at which the pooled ACF falls below e^{-1} . For the baseline rolling-median band [14, 20], finite-sample uncertainty is quantified by resampling the qualifying quiet episodes with replacement, which preserves within-episode serial dependence, and recomputing the pooled e-folding lag over 5000 bootstrap draws.

The field-stripped residual experiment uses the fitted M2 equilibrium path,

$$\epsilon_{\text{M2}}(t) = \psi_1(t) - \mu_{\text{eff}}(v_t), \quad (\text{B3})$$

computed on the same aligned sample. We compare the e-folding lag and the integrated ACF mass of raw ψ_1 and ϵ_{M2} over fixed horizons of 60 and 90 trading days. This pairing is intentional: the quiet regime removes field variation by sample restriction, whereas the residual experiment removes the fitted equilibrium path algebraically. Agreement between the two strengthens the attribution claim because it shows persistence collapse under two conceptually distinct manipulations.

4. Window sweep, non-overlapping reconstructions, auxiliary fields, and out-of-sample sweeps

The window sweep is conducted by recomputing ψ_1 from raw daily returns at five window lengths: $W = 30, 45, 60, 90, 120$. No smoothing approximation is used; each series is reconstructed from the returns and then aligned to the daily VIX field over the corresponding date range. At each W , M0 and M2 are fit from scratch and four outputs are retained: τ_0 , τ_{cond} , β/θ , and $\text{SCPA} = 1 - \tau_{\text{cond}}/\tau_0$. This protocol cleanly separates resolution dependence from code reuse, and it also provides an exact check that the $W = 60$ reconstruction reproduces the baseline order parameter.

To confront overlap directly, we also reconstruct disjoint weekly observables from 5-trading-day correlation matrices sampled every 5 trading days. This is done twice: once for a weekly ψ_1 proxy and once for weekly mean market correlation, both aligned to weekly VIX closes [38, 40]. For a same-horizon boundary check, we construct disjoint 60-trading-day blocks of ψ_1 and pair each block with either its end-of-block VIX level or its within-block mean VIX. These low-frequency series are intentionally retained even when underpowered, because their role is to show how much of the core attribution survives when measurement overlap is aggressively removed.

Auxiliary-field controls are run on the maximal same-sample intersections with the respective fields. MOVE is tested by fitting an OU+MOVE model and then a two-field OU+VIX+MOVE model on the intersection sample. TED is tested by fitting an OU+TED model on its own maximal intersection sample. The same BIC logic is used in every case. This design avoids misleading comparisons across unequal date ranges while still showing whether non-VIX fields carry independent dynamic information.

Out-of-sample evaluation is run at two levels. The baseline chronological holdout uses a single split at 2016-01-01. Parameters are estimated on the pre-2016 sample and scored on the post-2016 sample with the same exact one-step Gaussian likelihood. We report the average log likelihood on train and test and their ratio. Because the test set includes the COVID-19 period, the holdout is meaningfully harder than a random split and therefore functions as a basic stability stress test for the conditional field-proxy claim. As a sensitivity check, we also exclude 2020-03-01 through 2020-09-30 from the test period and score the pre- and post-COVID test segments separately, so that no one-step increment is evaluated across the excluded gap.

To avoid hinging on one split, we then run an anchored sweep with cut dates at 2010-01-01, 2012-01-01, 2014-01-01, 2016-01-01, 2018-01-01, and 2020-01-01. For each split, M0 and M2 are fit on the available prefix and scored on the entire held-out suffix under the same exact one-step Gaussian likelihood. The reported outputs are the M2 and M0 test log likelihoods per observation, the M2–M0 test gap, and the M2 test/train ratio. This design does not convert the problem into independent folds, but it does show whether the field-coupled advantage survives repeated chronological re-estimation.

5. Two-dimensional hidden-variable protocol and residual-state test

The 2D hidden-variable protocol is run first on the daily aligned $(\psi_1, \log \text{VIX})$ series and then on two Wand-faithful weekly reconstructions. In each dataset we fit three exact linear-Gaussian models: decoupled, feedforward, and bidirectional. The comparison is based on exact Gaussian likelihood and BIC. When the bidirectional model wins, we compute the projected kernel amplitude and timescale implied by the fitted continuous-time matrix. The stage gate is not whether any bidirectional model exists, but whether the observed VIX yields both bidirectional preference and a projected timescale compatible with the generalized-Langevin benchmark. That is why the daily, weekly-thinning, and Wand-faithful reconstructions are all retained.

The residual-state test uses the orthogonalized level residual ϵ_{\perp} rather than the mechanistic residual ϵ_{M2} . After splitting the $(\log \text{VIX}, \epsilon_{\perp})$ plane into four quadrants, we perform a focused forecasting comparison between Q2 and Q3 because that contrast captures the only genuinely operational claim proposed during manuscript development: conditional on low VIX, does a positive orthogonal residual predict a larger future increase in VIX than a negative one? We report mean future changes, Mann–Whitney p -values, and rank-biserial effect sizes at 30, 60, and 90 days. The design is intentionally narrow so that the result is either a clean positive or a clean negative rather than a diffuse narrative about state-space geometry.

TABLE IV. Exact window-size robustness of M0 and M2, recomputing ψ_1 directly from raw returns at each window. SCPA denotes $1 - \tau_{\text{cond}}/\tau_{\text{auto}}$.

W	θ_0	τ_0	θ	τ_{cond}	β	β/θ	SCPA	ΔBIC
30	0.00955	104.67	0.02927	34.17	0.00982	0.336	0.674	104.0
45	0.00553	180.79	0.02093	47.78	0.00706	0.337	0.736	99.4
60	0.00335	298.10	0.01640	60.99	0.00572	0.349	0.795	109.0
90	0.00194	516.68	0.01317	75.93	0.00488	0.370	0.853	153.6
120	0.00119	838.72	0.01036	96.55	0.00390	0.376	0.885	165.4

TABLE V. M2 fits with actual, mechanical-only, and informational-only fields on the decomposition sample.

Field	θ	τ_{cond}	β	$\Delta\text{BIC vs M0 (decomp. sample)}$
Actual log(VIX)	0.01723	58.05	0.00623	108.6
Mechanical-only proxy	0.00393	254.18	0.00026	-8.3
Informational residual	0.00850	117.67	0.00471	78.6

TABLE VI. Sensitivity of the mechanical/informational decomposition to volatility-freezing and weighting choices. The static split is recipe dependent, but the standalone dynamic conclusion is invariant across all tested variants.

Recipe	Mechanical fraction	Informational fraction	$\Delta\text{BIC mech-only}$	$\Delta\text{BIC info-only}$
Median freeze, equal weights	0.773	0.227	-8.35	78.59
Mean freeze, equal weights	0.776	0.224	-8.36	78.73
Pre-2016 median freeze, equal weights	0.779	0.221	-8.34	78.62
Median freeze, inverse-volatility weights	0.815	0.185	-8.27	77.71
Median freeze, volatility-share weights	0.721	0.279	-8.38	79.57

TABLE VII. One-dimensional non-overlapping robustness checks. The disjoint weekly reconstructions preserve strong support for M2, whereas same-horizon 60-day block reconstructions are retained only as low-power boundary checks.

Construction	n_{obs}	$\Delta\text{BIC M2 vs M0}$	τ_0 (trading days)	τ_{cond} (trading days)	SCPA
Daily overlapping baseline	4973	109.0	298.10	60.99	0.795
Disjoint weekly ψ_1	976	151.2	8.24	5.88	0.286
Disjoint weekly mean correlation	976	140.1	8.43	6.05	0.282
Disjoint 60-day blocks, end-of-block VIX	77	1.7	89.48	64.69	0.277
Disjoint 60-day blocks, block-mean VIX	77	-3.4	89.48	75.05	0.161

TABLE VIII. Anchored chronological out-of-sample sweep. For each split date, M0 and M2 are fit on the pre-split prefix and evaluated on the full held-out suffix.

Split date	n_{train}	n_{test}	M0 test ll/obs	M2 test ll/obs	M2-M0 test gap	M2 test/train ratio
2010-01-01	1451	3522	3.1931	3.2000	0.0070	0.964
2012-01-01	1955	3018	3.2227	3.2373	0.0146	0.994
2014-01-01	2457	2516	3.2294	3.2437	0.0143	0.999
2016-01-01	2961	2012	3.2219	3.2346	0.0128	0.995
2018-01-01	3464	1509	3.1653	3.1805	0.0152	0.972
2020-01-01	3967	1006	3.2301	3.2324	0.0023	0.995

TABLE IX. Quiet-regime band sensitivity. The strict daily band [15, 18] with a 120-trading-day minimum yields zero qualifying segments over 2004–2023. For the baseline rolling-median band [14, 20], the quiet e-folding estimate of 27 days carries an episode-bootstrap 95% confidence interval of [18, 33] days.

Rolling-median VIX band	Segments $\geq 120\text{d}$	Quiet e-folding lag	Full-sample e-folding lag
[13, 21]	5	27	69
[14, 20]	3	27	69
[15, 19]	0	—	69

TABLE X. Parameters of the constrained regime-switching plus VIX model M_RS,c+VIX on the aligned daily sample.

Parameter or derived quantity	Estimate
θ	0.02348
μ_{calm}	-0.6021
μ_{stress}	1.0000
β	0.00781
σ	0.00818
$p_{\text{calm} \rightarrow \text{stress}}$	0.01170
$p_{\text{stress} \rightarrow \text{calm}}$	0.8940
Expected calm duration (days)	85.5
Expected stress duration (days)	1.12
Stationary calm probability	0.9871
Stationary stress probability	0.0129
Calm-state relaxation time (days)	42.6

TABLE XI. Exact two-dimensional model comparisons and projected-kernel timescales across the daily and Wand-faithful datasets. The reported ΔBIC values are relative to the winning model in each panel.

Dataset	Winning structure	ΔBIC vs next-best	ΔBIC vs decoupled	Kernel timescale (days)
Daily aligned ψ_1	Feedforward	2.44	125.26	36.46 (full model only)
Naive weekly thinning	Feedforward	4.17	74.45	9.10 (full model only)
Wand-faithful weekly ψ_1	Bidirectional	0.78	154.10	33.47
Wand-faithful weekly mean correlation	Bidirectional	2.69	143.87	36.46

Appendix C: Supplementary Quantitative Tables

-
- [1] M. Scheffer, J. Bascompte, W. A. Brock, V. Brovkin, S. R. Carpenter, V. Dakos, H. Held, E. H. van Nes, M. Rietkerk, and G. Sugihara, *Nature* **461**, 53 (2009).
 - [2] E. A. Allen, E. Damaraju, S. M. Plis, E. B. Erhardt, T. Eichele, and V. D. Calhoun, *Cerebral Cortex* **24**, 663 (2014).
 - [3] R. Friedrich, J. Peinke, M. Sahimi, and M. Reza Rahimi Tabar, *Physics Reports* **506**, 87 (2011).
 - [4] R. Zwanzig, *Nonequilibrium Statistical Mechanics* (Oxford University Press, 2001).
 - [5] H. Risken, *The Fokker-Planck Equation: Methods of Solution and Applications* (Springer, 1996).
 - [6] C. W. Gardiner, *Stochastic Methods: A Handbook for the Natural Sciences and Engineering* (Springer, 2009).
 - [7] S. K. J. Falkena, C. Quinn, and J. Sieber, *Proceedings of the Royal Society A: Mathematical, Physical and Engineering Sciences* **475**, 20190075 (2019).
 - [8] J. Theiler, S. Eubank, A. Longtin, B. Galdrikian, and J. D. Farmer, *Physica D: Nonlinear Phenomena* **58**, 77 (1992).
 - [9] H. White, *Econometrica* **50**, 1 (1982).
 - [10] R. E. Kass and A. E. Raftery, *Journal of the American Statistical Association* **90**, 773 (1995).
 - [11] L. Laloux, P. Cizeau, J.-P. Bouchaud, and M. Potters, *Physical Review Letters* **83**, 1467 (1999).
 - [12] V. Plerou, P. Gopikrishnan, B. Rosenow, L. A. N. Amaral, and H. E. Stanley, *Physical Review Letters* **83**, 1471 (1999).
 - [13] V. Plerou, P. Gopikrishnan, B. Rosenow, L. A. N. Amaral, and H. E. Stanley, *Physical Review E* **65**, 066126 (2002).
 - [14] J. Bun, J.-P. Bouchaud, and M. Potters, *Physics Reports* **666**, 1 (2017).
 - [15] M. Potters and J.-P. Bouchaud, *A First Course in Random Matrix Theory for Physicists, Engineers and Data Scientists* (Cambridge University Press, 2020).
 - [16] G. Livan, M. Novaes, and P. Vivo, *Introduction to Random Matrices: Theory and Practice* (Springer, 2018).
 - [17] M. Billio, M. Getmansky, A. W. Lo, and L. Pelizzon, *Journal of Financial Economics* **104**, 535 (2012).
 - [18] M. Kritzman, Y. Li, S. Page, and R. Rigobon, *Journal of Portfolio Management* **37**, 112 (2011).
 - [19] K. J. Forbes and R. Rigobon, *Journal of Finance* **57**, 2223 (2002).
 - [20] G. Bekaert, C. R. Harvey, and A. Ng, *Journal of Business* **78**, 39 (2005).
 - [21] R. Cont, *Quantitative Finance* **1**, 223 (2001).
 - [22] R. Engle, *Journal of Business & Economic Statistics* **20**, 339 (2002).
 - [23] D. Sornette, *Why Stock Markets Crash: Critical Events in Complex Financial Systems* (Princeton University Press, 2003).
 - [24] T. Lux and M. Marchesi, *Nature* **397**, 498 (1999).
 - [25] R. Cont and J.-P. Bouchaud, *Macroeconomic Dynamics* **4**, 170 (2000).
 - [26] J.-P. Bouchaud, *Journal of Statistical Physics* **151**, 567 (2013).

- [27] M. Marsili and G. Raffaelli, *Advances in Complex Systems* **9**, 1 (2006).
- [28] P. Bak, C. Tang, and K. Wiesenfeld, *Physical Review Letters* **59**, 381 (1987).
- [29] J. P. Sethna, K. A. Dahmen, and C. R. Myers, *Nature* **410**, 242 (2001).
- [30] V. A. Marchenko and L. A. Pastur, *Matematicheskii Sbornik* **72**, 507 (1967).
- [31] M. C. Münnix, T. Shimada, R. Schäfer, F. Leyvraz, T. H. Seligman, T. Guhr, and H. E. Stanley, *Scientific Reports* **2**, 644 (2012).
- [32] H. K. Pharasi, K. Sharma, A. Chakraborti, K. Kaski, T. H. Seligman, V. Boginski, H. E. Stanley, and S. Jalan, *New Journal of Physics* **20**, 103041 (2018).
- [33] H. K. Pharasi, K. Sharma, A. Chakraborti, K. Kaski, T. H. Seligman, V. Boginski, H. E. Stanley, and S. Jalan, *Quantitative Finance* **20**, 1137 (2020).
- [34] M. Tumminello, F. Lillo, and R. N. Mantegna, *Journal of Economic Behavior & Organization* **75**, 40 (2010).
- [35] D. J. Fenn, M. A. Porter, M. McDonald, S. Williams, N. F. Johnson, and N. S. Jones, *Physical Review E* **84**, 026109 (2011).
- [36] D. Y. Kenett, M. Tumminello, A. Madi, G. Gur-Gershgoren, R. N. Mantegna, and E. Ben-Jacob, *PLoS ONE* **5**, e15032 (2010).
- [37] D.-M. Song, M. Tumminello, W.-X. Zhou, and R. N. Mantegna, *Physical Review E* **84**, 026108 (2011).
- [38] T. Wand, M. Heßler, and O. Kamps, *Entropy* **25**, 1257 (2023).
- [39] M. Heßler, T. Wand, and O. Kamps, *Entropy* **25**, 1265 (2023).
- [40] T. Wand, T. Wiedemann, J. Harren, and O. Kamps, *arXiv* (2023), [2309.12082](https://arxiv.org/abs/2309.12082).
- [41] P. Rinn, R. Schäfer, J. Kwapień, J. Peinke, and T. Guhr, *Europhysics Letters* **110**, 68003 (2015).
- [42] A. Stepanov, P. Rinn, T. Guhr, J. Peinke, and R. Schäfer, *Journal of Statistical Mechanics: Theory and Experiment* **2015**, P08011 (2015).
- [43] N. Bloom, *Econometrica* **77**, 623 (2009).
- [44] J. Driessen, P. J. Maenhout, and G. Vilkov, *Journal of Finance* **64**, 1377 (2009).
- [45] M. Gilson, E. Tagliacucchi, and R. Cofré, *Physical Review E* **107**, 024121 (2023).
- [46] J. D. Hamilton, *Econometrica* **57**, 357 (1989).
- [47] A. Ang and G. Bekaert, *Review of Financial Studies* **15**, 1137 (2002).
- [48] H. Y. Toda and T. Yamamoto, *Journal of Econometrics* **66**, 225 (1995).
- [49] B. LeBaron, *Quantitative Finance* **1**, 621 (2001).